β decay of ^{61}Mn to levels in ^{61}Fe

D. Radulov, C. J. Chiara, I. G. Darby, H. De Witte, J. Diriken, D. V. Fedorov, V. N. Fedosseev, L. M. Fraile, M. Huyse, U. Köster, B. A. Marsh, D. Pauwels, L. Popescu, M. D. Seliverstov, A. M. Sjödin, P. Van den Bergh, P. Van Duppen, M. Venhart, W. B. Walters, and K. Wimmer

Beta Decay of ^{61}Mn to levels in ^{61}Fe

D. Radulov,[1] C.J. Chiara,[2,3] I.G. Darby,[1] H. De Witte,[1] J. Diriken,[1,4] D.V. Fedorov,[5] V.N. Fedosseev,[6] L.M. Fraile,[7] M. Huyse,[1] U. Köster,[8] B.A. Marsh,[6] D. Pauwels,[1,4] L. Popescu,[4] M.D. Seliverstov,[1] A.M. Sjödin,[9] P. Van den Bergh,[1] P. Van Duppen,[1] M. Venhart,[1,10] W.B. Walters,[2] and K. Wimmer[11,12]

[1]*Instituut voor Kern- en Stralingsfysica, KU Leuven,*
Celestijnenlaan 200D, B-3001 Leuven, Belgium
[2]*Department of Chemistry and Biochemistry,*
University of Maryland, College Park, Maryland 20742, USA
[3]*Physics Division, Argonne National Laboratory, Argonne, Illinois 60439, USA*
[4]*Belgian Nuclear Research Centre SCK•CEN, Boeretang 200, B-2400 Mol, Belgium*
[5]*Petersburg Nuclear Physics Institute, RU-188300 Gatchina, Russia*
[6]*ISOLDE, CERN, CH-1211 Geneva 23, Switzerland*
[7]*Grupo de Física Nuclear, Universidad Complutense, 28040 Madrid, Spain*
[8]*Institut Laue Langevin, 6 rue Jules Horowitz, F-38042 Grenoble Cedex 9, France*
[9]*KTH-Royal Institute of Technology, SE-10044 Stockholm, Sweden*
[10]*Slovak Academy of Sciences, SK-84511 Bratislava, Slovakia*
[11]*Physik Department E12, Technische Universität München, D-85748 Garching, Germany*
[12]*Department of Physics, Central Michigan University, Mount Pleasant, Michigan 48859, USA*

A detailed beta-decay study of ^{61}Mn is presented, yielding extended information on the level structure of ^{61}Fe. Pure beams were obtained at ISOLDE, CERN, after selective laser ionization and mass separation of fission products from the bombardment of a UC$_x$ target by 1.4-GeV protons. The beta and gamma information was detected by two MiniBall clusters and three ΔE plastic scintillators. The new ^{61}Mn decay scheme reveals 48 gamma transitions, distributed over 20 excited states. A comparison to the decay scheme of ^{59}Mn and excited states in ^{59}Fe is made. Shell model calculations with two different interactions are performed in order to compare the nuclear structure of the two neighboring odd-A iron isotopes. Tentative spin and parities of several excited states in ^{61}Fe are assigned on the basis of beta decay feeding patterns in both ^{59,61}Fe and of results from the theoretical shell-model calculations.

I.   Introduction

The region of the nuclear chart around $Z = 28$ and $N = 40$ is particularly interesting since the discovery that, the first excited state in ^{68}Ni is a 0^+ state [1], the 2^+ energy locally peaks above 2 MeV [2] and the $B(E2)$ value locally minimizes in the nickel isotopes at $N = 40$ [3]. Especially the harmonic oscillator shell closure for neutrons at $N = 40$, separating the negative-parity pf and positive-parity $g_{9/2}$ orbitals, makes ^{68}Ni and adjacent nuclei objects of intensive studies, both experimentally [4–6] and theoretically [7, 8]. It has been suggested that neutron excitations across the $N = 40$ sub-shell closure, when moving to lighter Z-values below ^{68}Ni increases, resulting in the development of collective behavior as protons are removed from the $f_{7/2}$ single-particle orbital [9], making this region of the nuclear chart suitable for studying the effects of proton-neutron interactions and the onset of deformation [10, 11].
The iron nuclei, with two holes in the $Z = 28$ proton shell closure, are especially suited to study these effects. In contrast to the even-even nickel nuclei, where the first excited 2^+ state lies above 1 MeV reaching 2.034 MeV at $N = 40$, the first excited 2^+ state in the iron nuclei drives from 0.824 MeV in ^{60}Fe down to 0.522 MeV in ^{68}Fe. Only recently, were proper shell-model calculations able to describe the observed 2^+ excited states [12–14], at the cost of opening the pf neutron shell and introducing at least the $\nu g_{9/2}$ orbital in the calculations. In the odd-mass iron nuclei, the intrusion of the positive-parity $g_{9/2}$ neutron orbital into the pf shell leads to isomerism, which can be followed from ^{59}Fe on [15]. Even though partial experimental information on the neutron-rich even-even iron isotopes exists, above neutron number 36 it remains quite limited. Furthermore, only limited beta-decay information for manganese into odd-A iron is available. The lack, from ^{61}Fe on, of definitive spin assignments or even spin limitations, based on beta-decay feeding patterns, hinders a comparison to state of the art shell-model calculations.
Therefore an experimental campaign was set up at

ISOLDE, CERN to take advantage of the large and selective production of neutron-rich manganese isotopes, in order to bridge the gap between the well-studied manganese and iron isotopes near the stability line and the region around $N = 40$, through a systematic decay study using a dedicated beta-gamma detection set-up. In this article, the decay of ^{61}Mn to levels in ^{61}Fe is presented and compared to the well-studied ^{59}Mn to ^{59}Fe decay, where the ^{59}Fe levels have extensively been characterized through different studies including also spin-sensitive transfer reactions [16–19]. The striking similarity in beta-decay feeding for the two mass chains will be used to bring the spin assignments of the low-lying levels in ^{61}Fe onto a stronger footing. Using the powerful Z selectivity of the laser ionization, producing pure manganese sources, special attention will be paid to reliably obtain the ground-state feeding. Full details will be given on the experimental conditions of the measuring campaign, involving the decay chains ranging from ^{58,60}Mn to ^{68}Mn.

The data are compared to shell-model calculations that are performed with two widely used interactions in order to compare the nuclear structure in ^{59}Fe and ^{61}Fe.

II.   Experimental information on ^{61}Fe

Although the nucleus ^{61}Fe is close to the stability line, the information on its level scheme is quite limited. A beta-decay experiment on ^{61}Mn identified three excited states with energies 207, 391 and 629 keV [20]. The decay scheme was built on the basis of energy sum-relations and the time behavior of the intensity of the observed transitions. The ground state of ^{61}Mn was assigned $(5/2^-)$ [20] and a recent value of its half-life was reported to be $T_{1/2} = 0.62(1)$ s [10]. The beta-delayed neutron branching was determined to be 0.6(1)% of all ^{61}Mn decays [21]. The direct ground-state beta feeding of ^{61}Mn to ^{61}Fe was calculated, using time analysis of beta and gamma intensities from the decays of ^{61}Mn, its daughter, and granddaughter, and amounts to 74% [20]. The obtained $\log ft$ value of 4.4 for the ground state points to an allowed Gamow-Teller transition from $\nu f_{5/2}$ to $\pi f_{7/2}$ and restricts the spin and parity to $(3/2^-, 5/2^-)$. The most recent half-life value of the ground state of ^{61}Fe is reported to be 5.98(6) min [22], consistent with previous measurements. The excited state at 629 keV was previously identified as 620(20) keV [23] in a ^{64}Ni$(\alpha,^7$Be) reaction.

A new level with an isomeric character was identified in two reaction studies [24, 25]. Its energy was reported to be 862 keV and the measured half-life – $T_{1/2} = 0.22$ μs.

The existence of such a state, with a half-life of $T_{1/2} = 0.25(1)$ μs [15], was confirmed in a later fragmentation experiment, using an ^{86}Kr beam on a ^{nat}Ni target. It was proposed that its spin and parity are $(9/2^+)$, originating from the excitation of a neutron to the $g_{9/2}$ shell-model orbital. The state was found to decay to the previously observed excited state at 207 keV, with a transition of 654 keV. Because of its half-life, the transition was assigned an $(M2)$ multipolarity [15]. The $9/2^+$ spin and parity have been confirmed together with the multipolarities of the cascade transitions in two fragmentation experiments, aiming at measuring the magnetic and quadrupole moment of that state [26, 27], respectively. In both cases, ^{61}Fe was produced at GANIL in a reaction of ^{64}Ni on a ^{9}Be target. The extracted gyromagnetic factor in the former Ref.[26] is -0.229(2), consistent with shell-model calculations for a $9/2^+$ spin and parity. The half-life of the isomeric state was determined with a better precision: 239(5) ns [26]. The spectroscopic quadrupole moment was determined to be $|Q_s| = 41(6) e$fm^2 [27]. A perturbed angular distribution function analysis [27] concluded that the 207-keV transition has a $M1$ multipolarity, while the 654-keV one has $M2$. Prolate deformation was suggested for the isomeric state and possible excited states on top of it, analogous to experimental data for ^{57,59}Fe [28, 29]. The reduced transition probability, $B(E2)$, for the 207-keV line was determined in a Coulomb-excitation experiment to be 17(7) W.u. [30].

The yrast and near yrast structure of ^{61}Fe was revealed in two experiments [31, 32], using ^{64}Ni beams on ^{238}U targets at LNL, Legnaro and ANL, Argonne, respectively. In the first case, four transitions were observed. A transition of 752 keV, coincident with the 207 keV, defined an excited state at 959 keV, while two other transitions, a 788 keV and a 1341 keV, were found to be coincident with each other, but not with the former two gamma rays. It was proposed that the latter two defined yrast states above the known isomeric state and were interpreted as a coupling of the 2^+ and 4^+ states in ^{60}Fe with a $g_{9/2}$ neutron, which gives rise to states with spins and parities of $13/2^+$ and $17/2^+$, respectively [31]. It was noted that the observation of such a decoupled band, on top of the $9/2^+$ level, is consistent with a prolate deformation

of β_2=0.24, suggested for the isomeric state on the basis of the measured quadrupole moment and of mean-field calculations in [27]. In the second experiment, [32], new excited states were populated, while an angular-correlation analysis firmly set the multipolarities of many transitions, including the 655-207-keV cascade. The yrast states at 1650 and 2993 keV, built on top of the 862-keV level and decaying by the observed coincident transitions 789 and 1342 keV, have been assigned as $13/2^+$ and $17/2^+$ on the basis of angular correlations (see Fig.3 in [32]).

III.   Experimental set-up

In a measuring campaign at ISOLDE, CERN, radioactive $^{58,60-68}$Mn nuclei were produced in an induced fission reaction experiment, where 1.4-GeV protons impinged upon a UC$_x$ target (45 g/cm^2). The reaction products were selectively ionized by the laser ion source (RILIS [33]) using a three-step ionization scheme. The radioactive nuclei were accelerated over a 60-kV potential difference and mass separated on basis of their A/Q ratio, through the High-Resolution Separator [34]. The manganese beam was implanted on an aluminized mylar tape, inside a movable tape station ([35]) surrounded by three plastic ΔE beta detectors and two MiniBall [36] gamma-detector clusters in close geometry, as schematically shown in Fig.1.

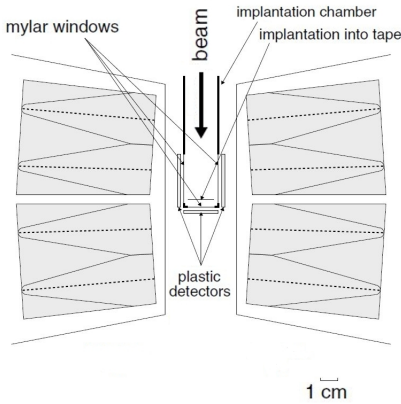Lead-brass-copper shielding was used to cover

FIG. 1. Schematic representation of the experimental set-up - top view [35].

the germanium detectors in order to decrease the gamma- and X-ray background. A polyethylene-borax shielding was built around the entire set-up to minimize the effect of neutron-induced gamma radiation at the detection station. The two shielding methods brought the background count rate of the germanium detectors down to around 50 Hz for all six cores, with protons on target. The germanium detectors were energy and efficiency calibrated, after the experiment, using ^{60}Co, ^{133}Ba, ^{241}Am, and ^{152}Eu gamma sources. The sources, with known intensities, were placed at the implantation site on the aluminized mylar tape. A full GEANT4 simulation was performed to correct the intensities of the gamma transitions from ^{60}Co and ^{152}Eu calibrations sources, in order to account for summing effects [37]. The photo-peak gamma efficiency for an energy of 1332 keV is 5.8(1)%.

The beta efficiency (ε_β) can be determined for each experimental decay set. It is defined as the ratio between the number of counts in a set of gamma-ray transitions in the beta-gated, prompt gamma spectrum, to the number of counts for these selected transitions in the singles gamma spectrum. The prompt coincidence time window for beta-gamma coincidences is from 0 to 600 ns, with respect to a beta event, while the prompt window for gamma-gamma coincidences is from -700 to +700 ns. The large prompt windows are due to digitization. Previous experiments indicate that the expectation value for ε_β is around 50% [35]. The information from the middle beta detector was not recorded in the A = 61 experimental data. A weighted mean value of 23.8(2)%, was obtained for the two side detectors in this decay set.

The experimental data were recorded on an event-by-event basis using digital electronics, with no hardware trigger applied. The trigger-less recording provides the flexibility for off-line sorting of the data, allowing for the setting of gates outside of the prompt time windows to search for isomeric states. The acquisition of the decay data was based on the CERN proton super cycle structure. A super cycle (SC) contains up to 40 proton pulses (PP) with a certain sequence, distributed with a difference of 1.2 s between each of them. In the present case, the super cycle consisted of 33 proton pulses of which ISOLDE received 11, non-consecutive ones with numbers: 4, 6, 8, 10, 13, 18, 21, 23, 26, 28, and 31. After each PP a delay time of 10 ms was introduced before the separator beam gate of 5 ms was opened, to let the beam implant on the tape. The delay time was introduced to suppress the implantation of isobaric ^{61}Ga contaminant, which is surface ionized and is released very fast. The manganese ions are released slower,

still the length of the implantation beam gate was limited to 5 ms only not to overload the detectors. Due to the high count rate in the germanium detec-
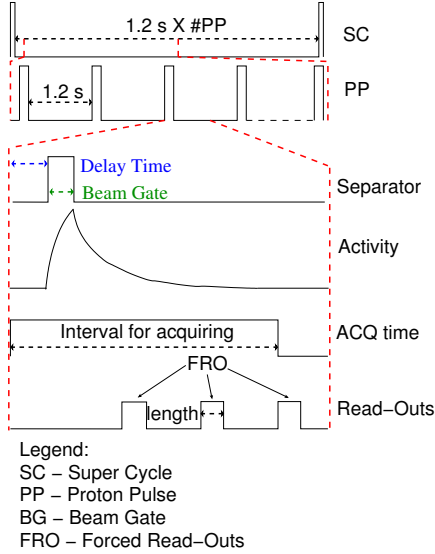

FIG. 2. (Color online) Schematic structure of the CERN proton super cycle and decay data taking. In this data set, the delay time was 10 ms and the implantation time was 5 ms. Two forced read-outs were used during the 1-s acquisition time and third one at the end. The read-outs were set at 250 and 650 ms after the PP, with a length of 150 ms.

tors, controlled forced read-outs of the digital buffers were used in order to allow for a proper fit of the ^{61}Mn half-life by requesting the read-outs at precise times during the acquisition time. Two read-outs were set at 250 and 650 ms after each PP signal, with a length of 150 ms. An overview of the measuring cycle is given in Fig.2. Before a new SC starts, the tape is moved and a new implantation-decay cycle begins.

IV. Results

Decay data corresponding to a total measuring time of 1531 s with the lasers set on resonance for manganese ionization and 170 s without lasers (Laser-off) were recorded. The dead time of the acquisition system was determined with the aid of a pulser in a channel of the digital ADC, set to a frequency of 100 Hz.

Laser ionization provides a clean and efficient method for selecting radioactive isotopes of interest.

In combination with a proper implantation-decay time structure and high-resolution mass separation, exceptional measurement conditions can be achieved with a source purity of almost 100%, as in the case of ^{61}Mn. This enables the possibility to follow the decay of the respective daughters and draw conclusions on the completeness of the decay schemes, addressing missed gamma-ray intensity and direct ground-state feeding.

A representative picture of the quality of the data in singles is shown in Fig.3, where all of the visible transitions were identified as following the decay of ^{61}Mn and its daughter (the very low background conditions in the experiment can be appreciated in the laser-off singles spectrum, drawn in red).
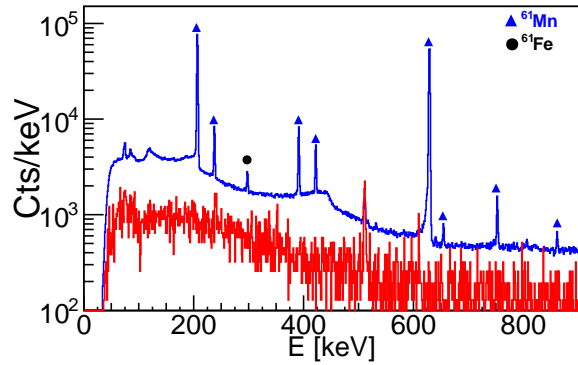

FIG. 3. (Color online) Singles γ-spectrum when the separator was set to mass 61. Lasers-on (in blue) is compared to a Laser-off spectrum (red – scaled for visual comparison) in the same experimental conditions. Triangles indicate ^{61}Mn lines, while the circle indicates a line following ^{61}Fe decay.

A. Half-life and beta-delayed neutron branch

The structure of the data taking allowed for the determination of the half-life of ^{61}Mn, as well as for the identification of new transitions in ^{61}Fe following the decay of ^{61}Mn, through their decay behavior. The intensities of the strongest gamma transitions following ^{61}Mn decay, in different time periods with respect to the PP signal (Fig.4), were fitted with an exponential decay function. The fits yield a weighted average value of $T_{1/2} = 0.708(8)$ s for the half-life of ^{61}Mn, in agreement with the value adopted by NNDC – $T_{1/2} = 0.67(4)$ s [38].

An upper limit for the beta-delayed neutron branching of ^{61}Mn to the first-excited state in ^{60}Fe was
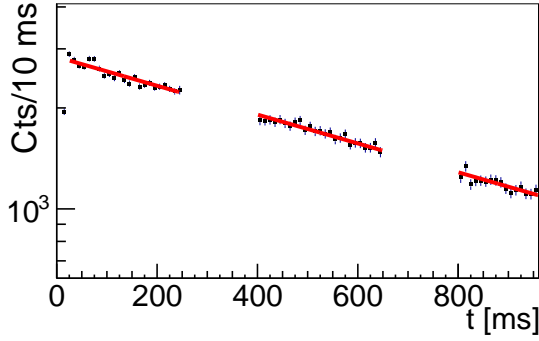
FIG. 4. (Color online) Exponential decay fit on the time behavior of the 629-keV transition. Each point contains the integrated number of counts in the peak area. Points inside the time intervals 0-20 ms (implantation of the radioactive ions), 250-400 ms (forced read-out) and 650-800 ms (forced read-out), are omitted from the fit.
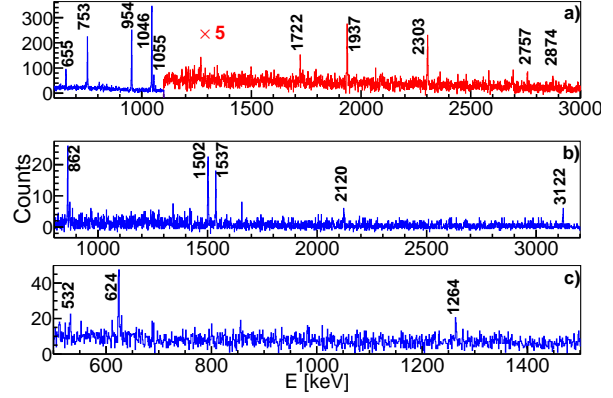

FIG. 5. (Color online) Prompt gamma-gamma-coincidence spectrum, gated on (a) the 207-keV, (b) the 391-keV, and (c) the 629-keV transitions. The energies of the strongest coincident transitions are indicated in keV.

determined using the upper limit of the number of counts in the area of the 824-keV $(2^+ \rightarrow 0^+)$ transition in ^{60}Fe, as this line was not observed in singles. From this, the limit for the direct beta-delayed neutron feeding to this excited state is deduced to be $P_n \leq 0.2\%$. The total beta-delayed neutron branch could not be determined due to the long half-life of ^{60}Fe $(T_{1/2} = 1.5 \times 10^6$ y [38]).

Hannawald [21] reported a total P_n value of 0.6(1)%. In view of the narrow window between the Q_β value of 7.18 MeV [39] and the neutron separation energy (S_n) of 5.58 MeV [38], the two values could be consistent. Hence, a value of $P_n = 0.6(1)\%$ is used further on.

B. Decay scheme

In order to build the decay scheme of ^{61}Mn, gamma-gamma coincidence gates were placed on the lines identified, through their half-life, as belonging to ^{61}Mn decay. The intensities of the weak transitions, not observed in singles, but observed in coincidence with a strong transition in ^{61}Fe, were calculated using the coincidence data. Example coincidence spectra, gated on the three strongest transitions in the decay, are presented in Fig.5. The analysis of the decay data revealed 48 gamma transitions, distributed over 20 excited states in ^{61}Fe.

The isomeric $9/2^+$ level at 862 keV was observed in this decay study, evidenced by the observation of the 655-207-keV cascade in beta-triggered delayed-gamma coincidence. A combination of two spectra with different time gates is shown in Fig.6. A subtraction remnant of the strongest transition in ^{61}Fe is visible next to the 655-keV transition.
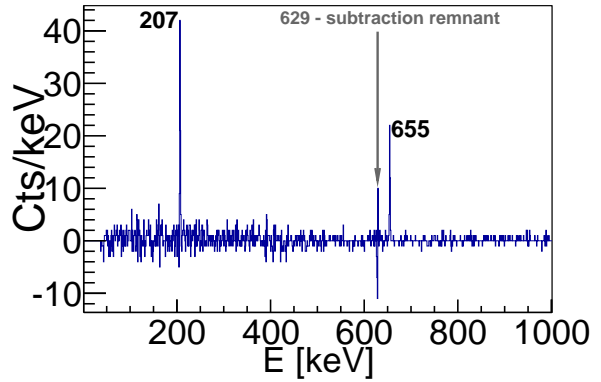

FIG. 6. (Color online) The decay of the 239(5)-ns, $9/2^+$ isomer. Selected part of the beta-triggered delayed-gamma spectrum with conditions: gamma-rays in 700 – 1420 ns time interval with respect to a beta-event (outside the prompt window); subtracted is a spectrum in the time interval 2500 – 3220 ns (randoms).

Making use of the high purity of the produced ^{61}Mn sources it is possible to connect the intensities of all placed gamma transitions in the mother decay to the intensities of the placed gamma transitions in the daughter decay. For certain cases in

5

this region of the nuclear chart, the decay chains can be quite complicated, due to the short half-lives and also the beta-delayed neutron decay channel can be important. The intensity balance is a strong test for judging the completeness of the obtained decay schemes and for determining the amount of direct beta feeding towards the ground state or the amount of missed ground-state gamma rays. Before a complete intensity balance can be made, and thus the absolute branching ratios deduced, it is convenient to define a new coefficient α for each beta-decaying state in the decay chain. It is the ratio between the intensity of the strongest ground-state gamma transition feeding the beta-decaying state, relative to the sum of the intensities of all identified ground-state transitions. In the case of the beta decay of ^{61}Mn, the strongest transition is the 629-keV line and the calculated coefficient is $\alpha_{Mn} = 55(1)\%$. Two methods were used to calculate the (beta and/or missed gamma) ground-state feeding in ^{61}Fe. In the first method, the decay information from the whole acquisition cycle is used, thus including the decay of ^{61}Fe in addition to the decay of ^{61}Mn. No direct beta feeding from the $(3/2^-, 5/2^-)$ ground state of ^{61}Fe to the $7/2^-$ ground state of ^{61}Co has previously been observed [40]. Using the normalization factor adopted in the NNDC evaluation to obtain the absolute intensity per 100 decays (0.436 ± 0.045 [38, 41]), the α_{Fe} value for the 1027-keV ($3/2^- \rightarrow 7/2^-$, Iγ = 98(5) [22]) ground-state transition, becomes 43(5)%. A simplified scheme of the $A = 61$ decay chain can be seen in Fig.7. The beta-delayed neutron branch of ^{61}Mn is adopted to be 0.6(1)% and can be ignored in the calculation. The apparent number of ^{61}Mn and ^{61}Fe decays, based on gamma detection, is calculated using the efficiency-corrected number of counts of, respectively, the 629- and 1027-keV transitions in singles, and the α_{Mn} and α_{Fe} coefficients. Using the measured beta efficiency of the ΔE plastic scintillators [$\varepsilon_\beta = 23.8(2)\%$], the total number of manganese plus iron decays, based on beta radiation, can also be extracted. The feeding of the ^{61}Fe ground state, due to missed gamma rays or direct beta feeding, is then deduced out of the comparison of the number of ^{61}Mn and ^{61}Fe decays from beta- and gamma-rays, to be 33(1)%.

In the second method, only information of the first proton pulse in the super cycle is taken into account, in order to minimize the amount of ^{61}Fe decays. The beta-delayed neutron branch of ^{61}Mn is once again ignored for the calculation. A gamma spectrum with time constraints in the first proton pulse is created. Due to the long half-life of the ground state of ^{61}Fe, with respect to the acquisition time of 1 s, no transi-
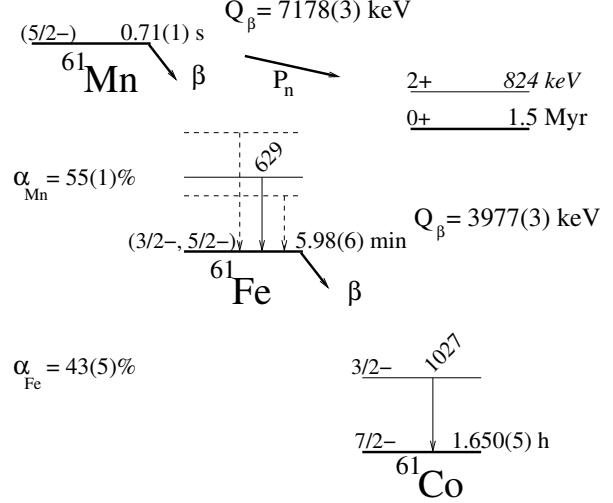

FIG. 7. Schematic representation of the $A = 61$ decay chain. All data but the half-life of ^{61}Mn and the calculated α_{Mn} are from Ref.[41], while the Q_β values are taken from Ref.[39].

tion following its decay is observed. This means that the intensity of the 629-keV line and its α_{Mn} factor can be used to calculate the apparent number of ^{61}Mn gamma decays and be compared to the number of decays from the beta counts. The obtained value for the missed feeding is 32(1)%. The agreement between the results obtained using the two methods shows that the relevant information on the decay chain of $A = 61$ (constructed decay scheme of ^{61}Mn and published decay scheme of ^{61}Fe) is consistent. The adopted value of 33(1)% is given in the decay scheme as the direct beta feeding to the ground state of ^{61}Fe, although one should realize that this is only an upper limit due to missed ground-state gamma transitions.

The direct beta-decay feeding of each excited level is calculated from the intensities of its feeding and de-exciting transitions and can be seen in Table I. Important to note here is the fact that the calculated beta-feeding listed in the latter table should be considered as upper limits, owing to the high Q_β value for that decay, even though several lines with energies above 2.5 MeV are observed, with relative intensities below 0.5% (see Table II). The complete ^{61}Mn decay scheme is presented in Fig.8, where the excited levels marked in red were observed in other experiments [15, 20, 32]. All gamma rays observed in this study as belonging to the decay of ^{61}Mn are given in Table II, together with the gamma rays in coincidence.

FIG. 8. (Color online) Decay scheme of ^{61}Mn, deduced from the present data. See Sec.V for discussion on the levels with assigned spins and parities. The Q_β value is from Ref.[39], P_n has been measured in [21], while the S_n and the half-lives of the ground and isomeric 862-keV states of ^{61}Fe are from [41].

7

E_{Level} (keV)	I_β (%)	$\log ft$	$T_{1/2}$
GS	33(1)	5.02(3)	5.98(6) m [22]
206.8	12.6(8)	5.38(3)	
391.2	< 0.28	> 7.3	
629.0	39.0(6)	4.77(1)	
861.5	< 0.22	> 7.1	239(5) ns [26]
959.5	0.49(7)	6.6(1)	
1013.0	< 0.30	> 7.0	
1160.9	3.23(9)	5.68(1)	
1252.8	3.25(9)	5.64(1)	
1262.3	0.57(6)	6.40(5)	
1477.2	< 0.17	> 7.3	
1705.1(5)	< 0.11	> 7.1	
1893.0	0.78(7)	6.04(4)	
1928.9	0.55(5)	6.18(4)	
2143.6	2.7(1)	5.40(2)	
2510.6	1.8(1)	5.43(2)	
2716.8	0.19(3)	6.32(7)	
2963.9(4)	0.13(2)	6.37(7)	
3049.1(2)	0.21(5)	6.12(11)	
3080.2(3)	0.22(5)	6.09(10)	
3513.3(4)	0.12(3)	6.14(11)	

TABLE I. Identified levels, their calculated beta-feeding intensities and $\log ft$ values in the decay of ^{61}Mn. The uncertainty on the level energy is better or equal to 0.1 keV, if not specified. Half-lives of the excited states are given, where information is available.

Following the presentation of preliminary results of this study at the ARIS-2011 conference, Waite et al. [42] reexamined the same deep-inelastic-scattering (DIS) data set used in Ref.[32] in the study of high-spin positive-parity levels that populate the $9/2^+$ level in ^{61}Fe. A general characteristic of DIS reactions is the population of yrast and near-yrast states; as the 207-keV, $(5/2^-) \rightarrow (3/2^-, 5/2^-)$ transition is yrast, double gates were systematically set on all transitions identified in this decay study as populating the level. Extensive high-spin structure was observed above the 1477-keV level and one additional transition was observed populating the 1161-keV level. This will further be used to narrow down the spin assignments.

V. Spin and parity assignments

Expected shell-model configurations for neutrons and protons, in this region, primarily involve the $\nu(p_{3/2}, f_{5/2}, p_{1/2}, g_{9/2})$ and $\pi(f_{7/2})$ orbitals, respectively. Having an even number of neutrons and with three proton holes in the $\pi f_{7/2}$ orbital, one would expect a $7/2^-$ ground state for the odd-A manganese

isotopes. The experimental information shows that this is not the case. In fact, the only isotope to exhibit such a spin and parity of its ground state is the neutron closed-shell nucleus ^{53}Mn$_{28}$ [38] (see Fig.9). One of the first attempts to describe the observed spins and parities of the ground states of the manganese isotopes was done in [43], in a model using a deformed representation of a single particle in the Nilsson orbitals coupled to a rotor. It was shown that this model describes significantly well the isotopes of ^{55,56}Mn. The ground state was calculated to be $5/2^-$ and a deformation of $\beta \sim 0.27$ was assigned to it. These experimental observations have been addressed also in the work of Paar [44], where a model that describes the excited states in a nucleus with three particles or holes outside a single-closed shell has been discussed. The calculated nuclei are represented as a three-hole cluster, coupled to the low-frequency quadrupole vibration of ^{58}Ni. The agreement in the description of the isotopes of ^{51,53,55}Mn was improved. The trend of $5/2^-$ spin-
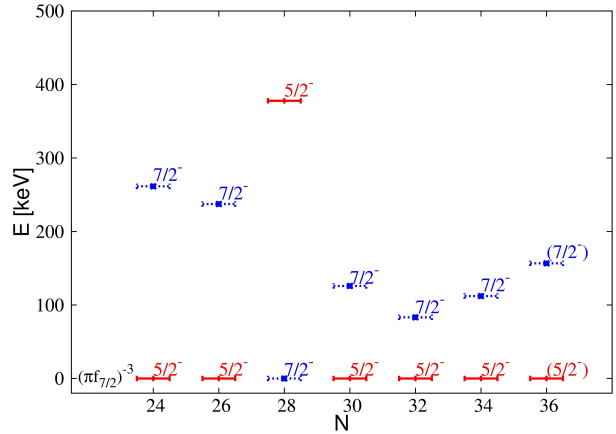

FIG. 9. (Color online) Systematics of the ground state and first excited state in odd-A $^{49-61}$Mn$_{24-36}$ isotopes [38, 45].

parity for the ground state and $7/2^-$ for the first-excited state is very well reproduced by recent shell-model (GXPF1A) calculations [46], where excellent agreement for the odd-mass $^{51-55}$Mn isotopes is obtained.

For the further spin and parity discussion, it is interesting to compare the obtained decay scheme of ^{61}Mn and the levels in ^{61}Fe with the information on the $A = 59$ decay chain.

The beta decay of ^{59}Mn has been investigated in Ref.[18]. Allowed beta transitions from the $5/2^-$ ^{59}Mn ground state were observed to the ground state
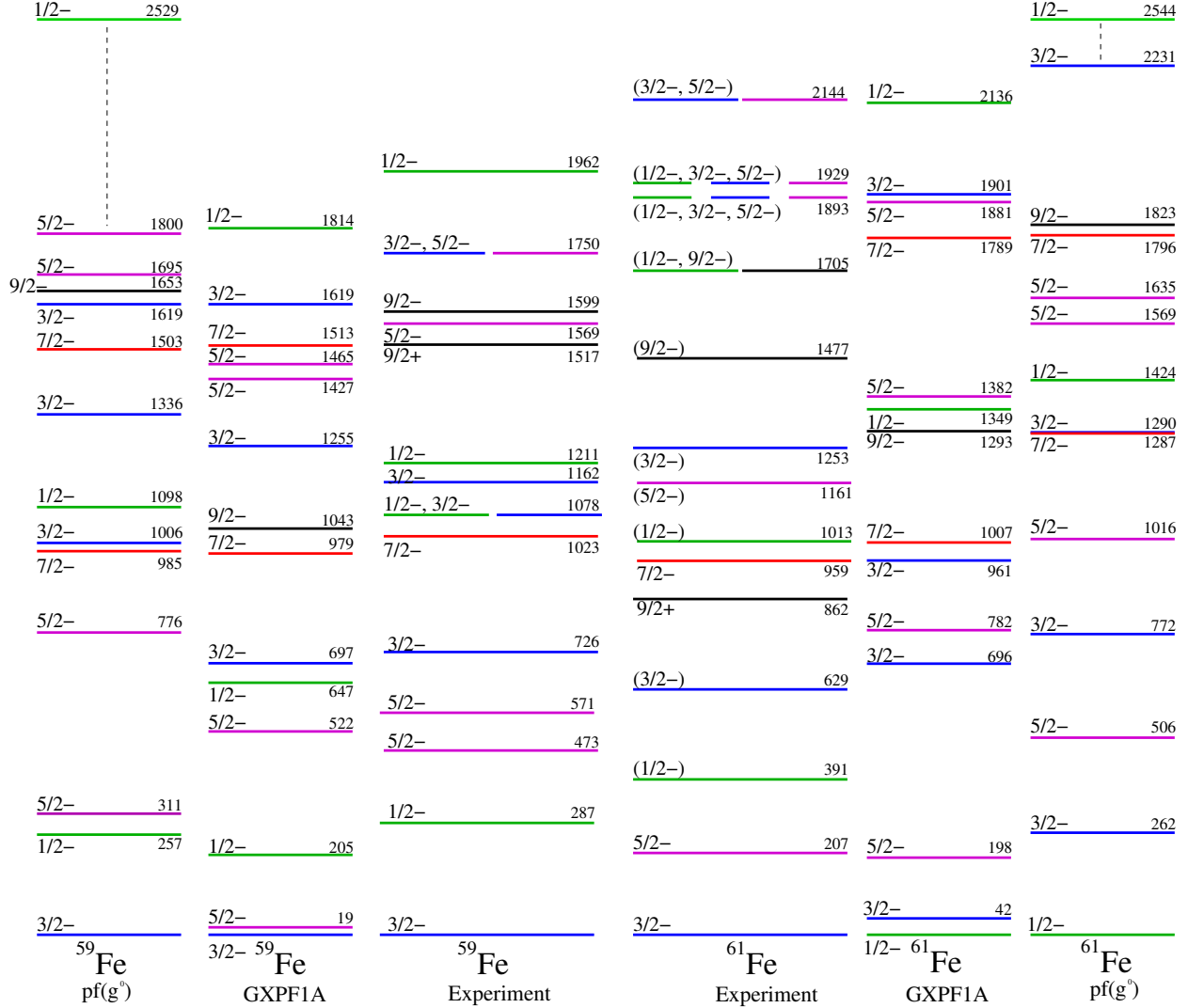
FIG. 10. (Color online) Comparison of the experimental data on the odd-A ^{59,61}Fe isotopes with shell-model calculations performed with two different interactions. Only negative-parity states are shown in the two experimental data sets with the exception of the $9/2^+$ excited state in both nuclei.

of ^{59}Fe and three low-lying excited states at 473, 571, and 726 keV. In a neutron-transfer experiment, ^{58}Fe$(d,p\gamma)^{59}$Fe [16], different states in ^{59}Fe were populated. Using the experimental cross-section distributions and DWBA calculations, the spin and parity assignments for most of them could be firmly fixed. Two states below 1 MeV were strongly populated, indicating their single-particle character – the ground state and the 473-keV level. This strong population was confirmed in a later (d,p) study [17]. Combining the beta-decay work [18], the transfer works [16] and [17], an (n,γ) work [47], and a fusion-evaporation study [19], leads to a number of firm spin and parity assignments of excited levels in ^{59}Fe, presented in Fig.10.

The situation concerning the spin and parity of the ground state of ^{61}Mn is not yet fully settled, as till now no direct measurement has been reported. Therefore, we keep the tentative $(5/2^-)$ assignment for its ground state. As the beta-decaying level of ^{61}Mn has such a spin and parity, direct, allowed and forbidden decays are possible to levels with spins 3/2, 5/2, and 7/2 in ^{61}Fe.

Seven strong beta transitions with $\log ft$ values be-

E_γ (keV)	Rel. Int. (%)	In observed coincidence with: (in keV)
201.6(5)*	0.24(4)	753
206.8(1)	54(2)	422, 655, 753, 807, 954, 1046, 1055, 1185, 1270, 1498, 1722, 1937, 2090, 2303, 2757, 2874
237.8(1)	4.61(6)	391
391.2(1)	7.37(9)	238, 862, 1502, 1538, 2120, 3122
422.2(1)	4.55(8)	207
517.9(5)*	0.12(4)	753
531.5(3)	0.15(4)	629
624.0(5)*	0.77(8)	629
629.0(1)	100	532, 624, 1264
640.5(3)	0.18(5)	1046, 1253
654.7(1)	0.56(6)	207
752.6(1)	1.89(6)	202, 207, 518, 1185, 2090
806.6(3)	0.21(5)	207
861.5(1)	0.49(5)	391
954.1(1)	2.88(9)	207
959.4(2)	0.43(12)	2090
982.4(5)*	0.22(8)	1161
1013.0(1)	1.30(7)	1131, 1498
1046.0(1)	4.49(9)	207, 641
1055.3(1)	1.05(7)	207
1130.6(1)	0.65(7)	1013
1161.0(1)	6.15(11)	982, 1351
1184.6(5)*	0.23(7)	207, 753
1239.7(1)	0.53(8)	1270
1252.9(1)	3.66(10)	641, 1259
1258.5(5)*	0.26(12)	1253
1262.7(1)	0.54(15)	—
1263.7(5)*	0.63(10)	629
1270.4(1)	0.71(15)	207, 1240, 1572
1350.8(5)*	0.31(10)	1161
1498.3(5)*	0.25(4)	207
1498.3(5)*	0.18(7)	1013
1501.7(1)*	0.76(9)	391
1537.7(1)	0.36(6)	391
1571.9(3)	0.24(7)	1270
1722.1(2)	0.29(6)	207
1893.9(3)	0.57(14)	—
1928.9(2)	0.86(12)	—
1936.8(1)	0.90(11)	207
2089.6(5)*	0.35(10)	207, 753, 959
2120.3(5)*	0.25(6)	391
2143.7(1)	5.54(14)	—
2303.5(1)	1.18(9)	207
2510.5(1)	2.86(12)	—
2757.4(5)*	0.37(7)	207
2873.7(3)	0.26(9)	207
3079.2(3)	0.34(10)	—
3122.1(4)	0.32(9)	391
1690.2(5)◇	0.19(6)	
1738.5(5)◇	0.15(6)	
1846.7(5)◇	0.16(5)	
3146.1(10)◇	0.26(10)	

TABLE II. Gamma transitions with their relative intensities, following the decay of ^{61}Mn, identified in this study together with gamma transitions observed in coincidence. The asterisk, "*", indicates that the transition was not seen in the singles spectrum, but its intensity was calculated using the coincidence data. The diamond, "◇", indicates unplaced transitions. For absolute intensity per 100 ^{61}Mn decays, multiply by 0.363(7).

low 5.7 are observed to the ground state, 207-, 629-, 1161-, 1253-, 2144- and 2511-keV levels, supporting firm negative-parity assignment for these levels (Table I). Comparing the measured $\log ft$ values with the published values for ^{59}Mn, a striking analogy between the two decay chains is apparent and a number of spin assignments can be inferred, supported by the preliminary analysis of the DIS data [42].

The similarity in direct ground-state feeding and the feeding to the 207-keV level, together with the decay pattern of the $9/2^+$ isomer (an $M2 - M1/E2$ cascade with no cross-over) fixes firmly the spin and parity of ^{61}Fe's ground state to $3/2^-$ and of the 207-keV state to $5/2^-$, confirming the results from the experiments noted in the introduction.

A tentative $(3/2^-)$ assignment is proposed for the 629-keV level, analogous to the 726-keV state in ^{59}Fe (Fig.10), based on the observed beta-decay feeding. A $(1/2^-)$ tentative assignment can be made for the 391-keV level in analogy to the 287-keV level in ^{59}Fe. The absence of strong beta-decay feeding and absence of feeding to that state in the DIS reaction supports such a spin and parity assignment for the 391-keV level. In particular, the lighter odd-mass $^{55-59}$Fe nuclei exhibit a $1/2^-$ level below 500 keV, hence the 391-keV level is the only candidate for such a state in this energy range in ^{61}Fe. Based on the latter conclusion for a $(1/2^-)$ spin and parity, all of the high-energy levels that decay into the 391-keV level, would be limited to spin and parity of $\leq 5/2^-$. The spin and parity of the excited state at 959 keV was determined to be $7/2^-$ following the angular-correlation analysis in Ref.[32].

The absence of any feeding in the DIS data suggests spins below 7/2 for the levels at 1013, 1253 and 1262 keV. The lowest of these can also be tentatively assigned as $(1/2^-)$ on the basis of the determined $\log ft$ of > 7, see Table I, while the strong beta branches for the levels at 1161 and 1253 keV rule out a $1/2^-$ assignment. Again, based on the analogy with levels in ^{59}Fe, where the second $5/2^-$ level is below the third $3/2^-$, the 1253-keV state can be tentatively assigned as $(3/2^-)$ and the one at 1161 keV as $(5/2^-)$ spin and parity.

In Ref.[32], a 517-keV transition was found to be coincident with the 752-207-keV cascade de-exciting the level at 959 keV, defining an excited state at 1477 keV (Fig.8). A $(5/2^-, 9/2^-)$ assignment is proposed based on the angular-correlation measurement in [32]. Information in the current decay work – the high $\log ft$ value and the lack of a transition to the ground state, can narrowed this down to $(9/2^-)$. The observations in [42], combined with the gamma-decay branching and the absence of strong beta de-cay towards that state as well as to the 862-keV state, are consistent with the proposed $(9/2^-)$ and the established $9/2^+$ spin and parity assignments, respectively. Due to the experimental conditions, though, it is not clear if the $9/2^+$ level at 862 keV is directly fed or through gamma decay from higher-lying levels.

The 1705-keV level in the beta decay of ^{61}Mn is fed with a $\log ft$ of > 7.1 (Table I). Its comparison with the values for the tentative $(1/2^-)$ at 391 keV and the $(9/2^-)$ at 1477 keV supports either of the spin and parity assignments for the former.

The beta feeding towards the state at 2144 keV suggests an allowed transition, thus spins and parities ranging from $(3/2^-)$ to $(7/2^-)$. Since no transition to the $7/2^-$ state at 959 is observed, a tentative $(3/2^-, 5/2^-)$ assignment is adopted in Fig.10.

VI. Discussion

An important feature of this study is the large amount of data collected and the likelihood that most, if not all, levels below 2 MeV with spins below 9/2 have been observed. Hence, the statement that the levels of ^{61}Fe are quite similar to those of ^{59}Fe can be made on the basis of finding the same amount of negative-parity levels up to ~ 2 MeV in both nuclei, presented in Fig.10. The strength of this statement is supported by the exhaustive data sets available for ^{59}Fe that still did not reveal any more levels in this energy range that would be populated in this beta decay study. In other words, this careful study has revealed neither a much larger nor a much smaller level density below that energy cut-off. Hence the question can be raised as to why the addition of two neutrons had so little impact on the observed structure. One answer is the rapid closure of the gap above which the $\nu g_{9/2}$ orbital lies. With a smaller gap, strong pairing provides for enhanced occupancy of the $\nu g_{9/2}$ orbital, leaving the negative-parity levels largely unperturbed. The strong pairing will keep the neutron pair in the $\nu g_{9/2}$ orbital from breaking in a way that can mix new configurations into the other low-spin negative-parity levels.

Two sets of shell-model calculations have been performed for negative-parity levels in ^{59,61}Fe for comparison with the experimental spectra of states in Fig.10. One set of levels was calculated with the code ANTOINE [48] using the GXPF1A [49] effective interaction with a ^{40}Ca core. The model space included protons and neutrons in the fp shell, although the $f_{7/2}$ neutron sub-shell was frozen with a full complement of eight neutrons, resulting in an

effective ^{48}Ca core. The other calculations were performed with the Oslo shell-model code [50], with the pfg interaction and a ^{48}Ca core as described in Ref.[51]. The model space includes protons in the fp shell and neutrons in the $p_{3/2}$, $f_{5/2}$, $p_{1/2}$, and $g_{9/2}$ orbitals; here, however, excitations into the $g_{9/2}$ neutron orbital were blocked. Thus, both calculations were performed in the same model space but with different two-body matrix elements and single-particle energies for the active fp orbitals.

Comparing with the model calculations, two features stand out: the inability of either model to place two $5/2^-$ levels close together in ^{59}Fe and the finding of $1/2^-$ ground-state spin and parity in both models for ^{61}Fe. Furthermore, the calculated levels for ^{59}Fe provide at least as good fit to the observed levels of ^{61}Fe as do the levels calculated with the addition of another pair of neutrons. This is especially pertinent, given that both calculations for ^{61}Fe show a $1/2^-$ spin and parity for the ground state.

The similarity of the levels in ^{59,61}Fe is also consistent with the nearly constant $B(E2)$ values up to ^{62}Fe, with a large jump observed for ^{64}Fe and ^{66}Fe [6], where the added occupancy of the $\nu g_{9/2}$ and/or the $\nu d_{5/2}$ orbital can polarize the nucleus to a much stronger degree [12, 13].

VII. Conclusion

A decay study of selectively produced ^{61}Mn has been performed, resulting in an extended decay scheme which resembles strongly the decay scheme of ^{59}Mn. Several new levels were found and, out of the analogy with the beta-decay of ^{59}Mn, the spin and parity assignments of the lowest-lying levels could be placed on more convincing grounds. A number of tentative spins and parities is proposed for higher-lying states based on the information in the current beta-decay study and the preliminary data from the deep-inelastic study by [42]. The new levels identified here for ^{61}Fe reveal an unexpectedly close similarity to the well studied levels of ^{59}Fe, especially when compared to shell-model calculations. One conclusion is that, in spite of the improved models and the large configuration spaces (full fp shell for protons and $f_{5/2}p$ shell for neutrons), neither of the models in widespread use that we have employed in this study is able to reproduce key features of the observed level structure. The new data on the decay of ^{61}Mn to levels in ^{61}Fe, combined with the rather complete high-spin structure known from different reaction studies for the level structure in ^{59}Fe, quite close to stability, can now be used for even more ex-

tended model calculations and as a benchmark for further studies, reaching towards the more neutron-rich odd-mass iron isotopes.

[1] M. Bernas, P. Dessagne, M. Langevin, J. Payet, F. Pougheon, and P. Roussel, Physics Letters B **113**, 279 (1982).

[2] R. Broda *et al.*, Phys. Rev. Lett. **74**, 868 (1995).

[3] O. Sorlin, S. Leenhardt, C. Donzaud, J. Duprat, F. Azaiez, F. Nowacki, H. Grawe, Z. Dombrádi, F. Amorini, A. Astier, D. Baiborodin, M. Belleguic, C. Borcea, C. Bourgeois, D. M. Cullen, Z. Dlouhy, E. Dragulescu, M. Górska, S. Grévy, D. Guillemaud-Mueller, G. Hagemann, B. Herskind, J. Kiener, R. Lemmon, M. Lewitowicz, S. M. Lukyanov, P. Mayet, F. de Oliveira Santos, D. Pantalica, Y.-E. Penionzhkevich, F. Pougheon, A. Poves, N. Redon, M. G. Saint-Laurent, J. A. Scarpaci, G. Sletten, M. Stanoiu, O. Tarasov, and C. Theisen, Phys. Rev. Lett. **88**, 092501 (2002).

[4] A. Dijon, E. Clément, G. de France, G. de Angelis, G. Duchêne, J. Dudouet, S. Franchoo, A. Gadea, A. Gottardo, T. Hüyük, B. Jacquot, A. Kusoglu, D. Lebhertz, G. Lehaut, M. Martini, D. R. Napoli, F. Nowacki, S. Péru, A. Poves, F. Recchia, N. Redon, E. Sahin, C. Schmitt, M. Sferrazza, K. Sieja, O. Stezowski, J. J. Valiente-Dobón, A. Vancraeyenest, and Y. Zheng, Phys. Rev. C **85**, 031301(R) (2012).

[5] C. J. Chiara, R. Broda, W. B. Walters, R. V. F. Janssens, M. Albers, M. Alcorta, P. F. Bertone, M. P. Carpenter, C. R. Hoffman, T. Lauritsen, A. M. Rogers, D. Seweryniak, S. Zhu, F. G. Kondev, B. Fornal, W. Królas, J. Wrzesiński, N. Larson, S. N. Liddick, C. Prokop, S. Suchyta, H. M. David, and D. T. Doherty, Phys. Rev. C **86**, 041304(R) (2012).

[6] W. Rother, A. Dewald, H. Iwasaki, S. M. Lenzi, K. Starosta, D. Bazin, T. Baugher, B. A. Brown, H. L. Crawford, C. Fransen, A. Gade, T. N. Ginter, T. Glasmacher, G. F. Grinyer, M. Hackstein, G. Ilie, J. Jolie, S. McDaniel, D. Miller, P. Petkov, T. Pissulla, A. Ratkiewicz, C. A. Ur, P. Voss, K. A. Walsh, D. Weisshaar, and K.-O. Zell, Phys. Rev. Lett. **106**, 022502 (2011).

[7] K. Langanke, J. Terasaki, F. Nowacki, D. J. Dean, and W. Nazarewicz, Phys. Rev. C **67**, 044314 (2003).

[8] D. Pauwels, J. L. Wood, K. Heyde, M. Huyse, R. Julin, and P. Van Duppen, Phys. Rev. C **82**, 027304 (2010).

[9] T. Otsuka, T. Suzuki, R. Fujimoto, H. Grawe, and Y. Akaishi, Phys. Rev. Lett. **95**, 232502 (2005).

[10] M. Hannawald *et al.*, Phys. Rev. Lett. **82**, 1391 (1999).

[11] N. Hoteling *et al.*, Phys. Rev. C **74**, 064313 (2006).

[12] E. Caurier *et al.*, Eur Phys. J. A **15**, 145 (2002).

[13] S. M. Lenzi, F. Nowacki, A. Poves, and K. Sieja, Phys. Rev. C **82**, 054301 (2010).

[14] J. Ljungvall, A. Görgen, A. Obertelli, W. Korten, E. Clément, G. de France, A. Bürger, J.-P. Delaroche, A. Dewald, A. Gadea, L. Gaudefroy, M. Girod, M. Hackstein, J. Libert, D. Mengoni, F. Nowacki, T. Pissulla, A. Poves, F. Recchia, M. Rejmund, W. Rother, E. Sahin, C. Schmitt, A. Shrivastava, K. Sieja, J. J. Valiente-Dobón, K. O. Zell, and M. Zielińska, Phys. Rev. C **81**, 061301(R) (2010).

[15] R. Grzywacz, R. Béraud, C. Borcea, A. Emsallem, M. Glogowski, H. Grawe, D. Guillemaud-Mueller, M. Hjorth-Jensen, M. Houry, M. Lewitowicz, A. C. Mueller, A. Nowak, A. Plochocki, M. Pfützner, K. Rykaczewski, M. G. Saint-Laurent, J. E. Sauvestre, M. Schaefer, O. Sorlin, J. Szerypo, W. Trinder, S. Viteritti, and J. Winfield, Phys. Rev. Lett. **81**, 766 (1998).

[16] K. C. McLean, S. M. Dalgliesh, S. S. Ipson, and G. Brown, NPA **191**, 417 (1972).

[17] T. Taylor and J. A. Cameron, Nucl. Phys. A **337**, 389 (1980).

[18] M. Oinonen *et al.*, Eur Phys. J. A **10**, 123 (2001).

[19] A. N. Deacon, S. J. Freeman, R. V. F. Janssens, M. Honma, M. P. Carpenter, P. Chowdhury, T. Lauritsen, C. J. Lister, D. Seweryniak, J. F. Smith, S. L. Tabor, B. J. Varley, F. R. Xu, and S. Zhu, Phys. Rev. C **76**, 054303 (2007).

[20] E. Runte *et al.*, Nucl. Phys. A **441**, 237 (1985).

[21] M. Hannawald, *Kernspektroskopie an N≃40 und N≃82 Nukliden*, Ph.D. thesis, University of Mainz (2000).

[22] J. Bron, H. W. Jongsma, and H. Verheul, Phys. Rev. C **11**, 966 (1975).

[23] J. D. Cossairt, R. E. Tribble, and R. A. Kenefick, Phys. Rev. C **15**, 1685 (1977).

[24] R. Broda, in *Proc. Int. Conf. Fiss. Prop. Neut.-Rich Nucl.* (1998).

[25] B. Fornal, *IFJ Cracow Annual Report*, Tech. Rep. (IFJ, 1994).

[26] I. Matea *et al.*, Phys. Rev. Lett. **93**, 142503 (2004).

[27] N. Vermeulen, S. K. Chamoli, J. M. Daugas, M. Hass, D. L. Balabanski, J. P. Delaroche, F. de Oliveira-Santos, G. Georgiev, M. Girod, G. Goldring, H. Goutte, S. Grévy, I. Matea, P. Morel, B. S. N. Singh, Y.-E. Penionzkevich, L. Perrot, O. Perru, S. Péru, O. Roig, F. Sarazin, G. S. Simpson, Y. Sobolev, I. Stefan, C. Stodel, D. T. Yordanov, and G. Neyens, Phys. Rev. C **75**, 051302(R) (2007).

[28] A. M. Nathan, J. W. Olness, E. K. Warburton, and J. B. McGrory, Phys. Rev. C **17**, 1008 (1978).

[29] E. K. Warburton, J. W. Olness, A. M. Nathan, J. J. Kolata, and J. B. McGrory, Phys. Rev. C **16**, 1027 (1977).

[30] J. Van de Walle *et al.*, Eur Phys. J. A **42**, 401 (2009).

[31] S. Lunardi *et al.*, Phys. Rev. C **76**, 034303 (2007).

[32] N. Hoteling *et al.*, Phys. Rev. C **77**, 044314 (2008).

[33] V. N. Fedosseev *et al.*, Rev. of Sci. Instrum. **83**, 02A903 (2012).

[34] B. Riisager and K. Jonson, Scholarpedia **5**, 9742 (2010).

[35] D. Pauwels *et al.*, Nucl. Instr. and Meth. Phys. Res. B **266**, 4600 (2008).

[36] J. Eberth *et al.*, Prog. in Part. and Nucl. Phys. **46**, 389 (2001).

[37] M. Venhart, "Private communications,".

[38] ENSDF, www.nndc.bnl.gov/ensdf/.

[39] M. Wang, G. Audi, A. Wapstra, F. Kondev, M. MacCormick, X. Xu, and B. Pfeiffer, Chinese Physics C **36**, 1603 (2012).

[40] D. Ehrlich, Z.Phys. **207**, 268 (1967).

[41] M. Bhat, Nuclear Data Sheets **88**, 417 (1999).

[42] M. Waite *et al.*, To be published.

[43] J. R. Comfort, P. Wasielewski, F. B. Malik, and W. Scholz, NPA **160**, 385 (1971).

[44] V. Paar, Nucl. Phys. A **211**, 29 (1973).

[45] XUNDL, www.nndc.bnl.gov/ensdf/ensdf/xundl.jsp.

[46] F. Charlwood, *Ground state properties of Mn and Mo using laser spectroscopic methods*, Ph.D. thesis, University of Manchester (2010).

[47] R. Vennink, J. Kopecky, P. Endt, and P. Glaudemans, Nuclear Physics A **344**, 421 (1980).

[48] E. Caurier and F. Nowacki, Acta Physica Plonica B **30**, 705 (1999).

[49] M. Honma, T. Otsuka, B. Brown, and T. Mizusaki, The European Physical Journal A - Hadrons and Nuclei **25**, 499 (2005).

[50] M. Hjorth-Jensen, T. T. S. Kuo, and E. Osnes, Physics Reports **261**, 125 (1995).

[51] N. Hoteling *et al.*, Phys. Rev. C **82**, 044305 (2010).